Int. J. Electrochem. Sci., 13 **(2018)** 7532 – 7544, doi: 10.20964/2018.08.37

International Journal of ELECTROCHEMICAL SCIENCE
www.electrochemsci.org

Properties of Gradient Multilayer Nickel Coatings Prepared by Interlaced Jet Electrodeposition

Mingzhi Fan[1], *Lida Shen*[1,*], *Mingbo Qiu, Zhanwen Wang, Zongjun Tian*

College of Mechanical and Electrical Engineering, Nanjing University of Aeronautics and Astronautics, No. 29 Yudao Street, Nanjing, Jiangsu 210016, PR China.
[1] These authors contributed equally to this work.
[*]E-mail: ldshen@nuaa.edu.cn

Received: 4 May 2018 / *Accepted:* 8 June 2018 / *Published:* 5 July 2018

Jet electrodeposition is an effective method to prepare protective coatings on NdFeB. To improve the performance of interlaced multilayer coatings, layers that changed periodically and gradiently were prepared by changing the current density for even layers. The surface morphology and microstructure of the coatings were characterized by scanning electron microscopy and X-ray diffraction. The adhesion strength, microhardness, and corrosion resistance of the coatings were measured using an automatic scratch tester, a microhardness tester, and an electrochemical workstation. The results indicated that compared with other coatings, the periodic gradient multilayer coatings obtained a flatter surface and a higher corrosion resistance. In addition, the adhesion strength was increased from 9.2N to 21.7N, and the microhardness was increased from 484HV to 539HV.

Keywords: Sintered NdFeB; Interlaced jet electrodeposition; Periodic gradient multilayer coating; Adhesion strength; Corrosion resistance

1. INTRODUCTION

The NdFeB permanent magnet is currently the most productive rare-earth permanent magnet material. It is widely used in consumer electronics, automotive industry, industrial energy-efficient motor, wind power devices, medical devices, and other industries [1–3]. Owing to the high chemical activity of neodymium and the multiphase structure of the NdFeB material, it is easily corroded in hygrothermal environment [4]. Alloying and protective coatings are the most frequently used methods to improve the corrosion resistance of the NdFeB material [5–8]. Mo found that magnets with MgO addition developed increased resistance to humid environments [5]. Ali prepared a titanium nitride coating on sintered NdFeB permanent magnets, which exhibited excellent protection against corrosion

[7]. Jet electrodeposition provides distinct advantages in the preparation of protective coatings because of its high limiting current density, fine crystallization, and compact deposition layer [9–12]. Shen demonstrated that the multilayered nickel coating has a considerably higher corrosion resistance than single-layer bright nickel or dark nickel [11]. Wang proposed a technique involving discontinuous cathode rotation and interlaced deposition, which improved the uniformity, adhesion strength, and corrosion resistance of the multilayer coatings on NdFeB substrate [12]. However, the effect of current density on Ni coating was not investigated.

As a type of functionally graded materials, the gradient multilayer coating (including gradient composition coating and gradient microstructure coating) has drawn academic interest. Various electrodeposition processes have been developed, and the properties of gradient multilayer coatings have been evaluated [13–15]. Wang prepared Ni–W alloy coatings with low stress, high hardness, high mechanical strength, and high corrosion resistance by gradually increasing the bath temperature and cathode current density [13]. García-Lecina deposited a bright and compact composite coating by changing the concentration of SiC in the solution, which exhibited high hardness, good adhesion, and wear resistance [14]. However, these approaches have certain limitations. For example, coating components are difficult to control, and nanoparticles easily agglomerate.

Interlaced jet electrodeposition is a simple and easily controlled technique to prepare gradient multilayer coatings. Given the advantages of interlaced deposition and the effects of current density on the grain size and microstructure of the coating [9,10,16,18], periodic gradient multilayer nickel coatings were prepared by periodically changing the deposition direction and the deposition current density. During preparation, the current density used to plate even layers varied were different for different samples, whereas the current density used to plate odd layers remained unchanged. The effects of different current densities for even layers on the properties of the coatings on the NdFeB substrate were evaluated.

2. EXPERIMENTAL

2.1 Experimental equipment

Fig.1 presents the experimental equipment. The reciprocating translation of the anode is controlled by the x-axis motor, and the vertical movement of the anode is controlled by the z-axis motor. The rotation of the bevel gear is controlled by the y-axis motor, which causes the cathode to rotate cyclically. The spray nozzle, workpiece stage, and bevel gears are printed by a 3D printer. The scanning speed and scanning width of the nozzle, as well as the rotation angle of the cathode, are automatically controlled by the program. The anode chamber is filled with several nickel beads to enhance the conductivity and maintain the concentration of nickel ions in the solution. The temperature of the plating solution is controlled using a water bath. The flow is controlled by the valve of the flowmeter. The plating solution is pumped into the anode chamber from the plating bath and then sprayed through the nozzle onto the workpiece. Deposition begins as soon as power is turned on.

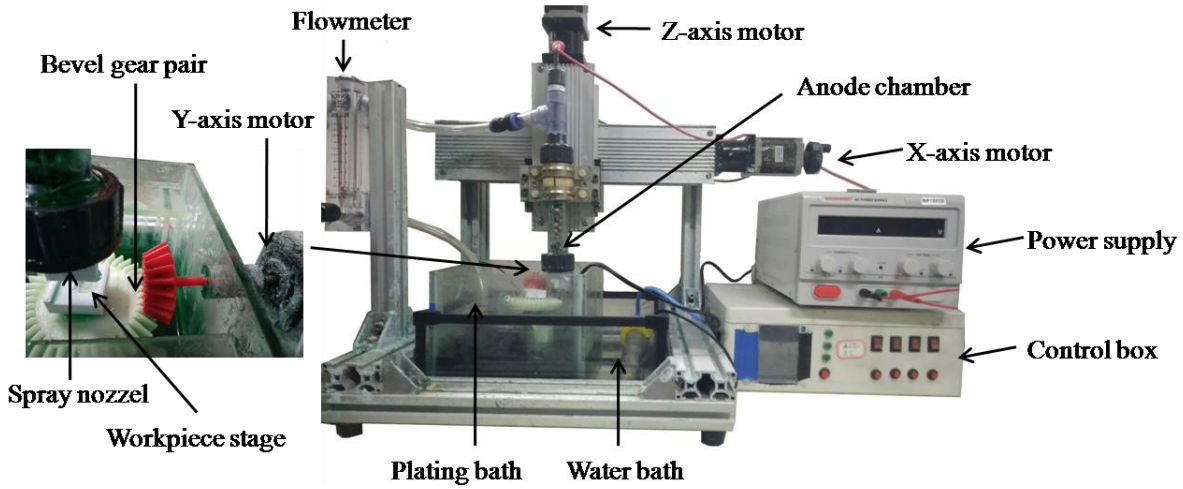

Figure 1. Experimental equipment

2.2 Pretreatment of substrate

Sintered N35 NdFeB measuring 20 mm ×20 mm × 2mm was selected as the substrate. The pretreatment process involved the following steps: manual grinding with 200#, 400#, 800#, and 1200# metallographic sandpaper→ polishing with a metallographic polishing machine(spray polishing agent containing 3.5 μm diamond particles)→ rinsing with deionized water → ultrasonic degreasing in alkaline solution(25°C, 2min)→ rinsing with deionized water→ ultrasonic cleaning in alcohol→ sealing with zinc stearate (30min) after drying→ slight polishing with a metallographic polishing machine→ ultrasonic cleaning in alcohol→ drying for use.

2.3 Experimental method

The deposit obtained during the reciprocating translation of the anode 14 times was considered as one layer. Fig.2 illustrates the deposition process. After the odd layer was deposited, the power was turned off, and the workpiece was rotated anticlockwise by 90°. The power was then turned on, and the even layer was deposited. Power was subsequently turned off, and the workpiece was rotated clockwise by 90°. The power was then turned on, and the next odd layer was deposited. Following this sequence, the final coating consisted of 21 layers. In this study, the current density for odd layers was maintained at 100A/dm^2. The effects of different current densities for even layers on the properties of the coatings on the NdFeB substrate were evaluated. The samples and the corresponding current density for even layers are listed in Table 1.The presence of additives in the bath can substantially change the property of the plating solution, thereby influencing the surface quality, microstructure, and properties of coatings [16,17]. Consequently, a Watt's solution without any additives was used in this study. The electrolyte composition and electrodeposition conditions of the experiment are listed in Table 2.

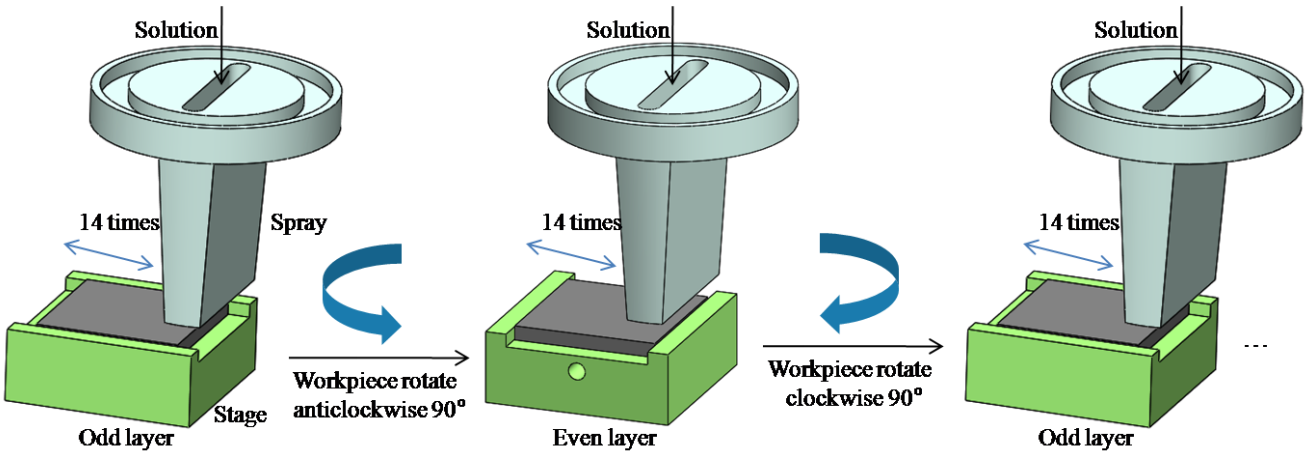

Figure 2. Schematic diagram of process

Table 1. Current density for even layers

Sample number	current density for even layers (A/dm^2)
1	60
2	100
3	140

Table 2. Solution components and processing conditions

Solution components and processing conditions	Value
$NiSO_4.6H_2O$	280 g/L
$NiCl_2.6H_2O$	40 g/L
H_3BO_4	40 g/L
Temperature	50°C
Rate of flow	220L/h

2.4 Test instruments

The surface morphology and cross-sectional morphology of the coatings on the NdFeB substrate were characterized by scanning electron microscopy (S-4800; Hitachi Instruments, Inc., Tokyo, Japan). The microstructure of the coatings was investigated by X-ray diffraction (DMAX-2500PC; Rigaku Corp., Tokyo, Japan) under the following conditions: 30°–80° diffraction angles, Cu-Kα radiation (λ= 1.5406 Å), 40kV, 100 mA, 0.02° step width, and 10°/min scanning speed. The microhardness was measured using a digital microhardness tester (HXS-1000AK; Bsida Instruments Co., Chengdu), operated with a load of 200g and a maintaining time of 10s. The adhesion strength was tested using an automatic scratch instrument (WS-2005; Zhongkekaihua Science and Technology Development Co., LanZhou), choosing the measurement method of friction force and the operating

mode of dynamic load. The corrosion resistance of the coatings was evaluated using an electrochemical workstation (CHI660E; Chenhua Instruments Co., Shanghai) with a 3-electrode system. The reference electrode used was the saturated calomel electrode, whereas the counter electrode was a platinum electrode. The exposed area of the samples was $1cm^2$. The potentiodynamic polarization curve with a scanning rate of 1mV/s and the electrochemical impedance spectra with frequencies ranging from 10^5Hz to 10^{-2}Hz were measured in a 3.5 wt% NaCl solution at room temperature.

3. RESULTS AND DISCUSSION

3.1 Surface morphology

Fig.3 presents the surface morphology of the coatings. Fig.3b reveals numerous bulges on the surface of the coating prepared at constant current density. When the current density for even layers was decreased to 60 A/dm^2, the number of bulges and the size of bulges decreased (Fig.3a). When the current density for even layers was increased to 140 A/dm^2, the coating surface appeared flat with almost no bulges present (Fig.3c).

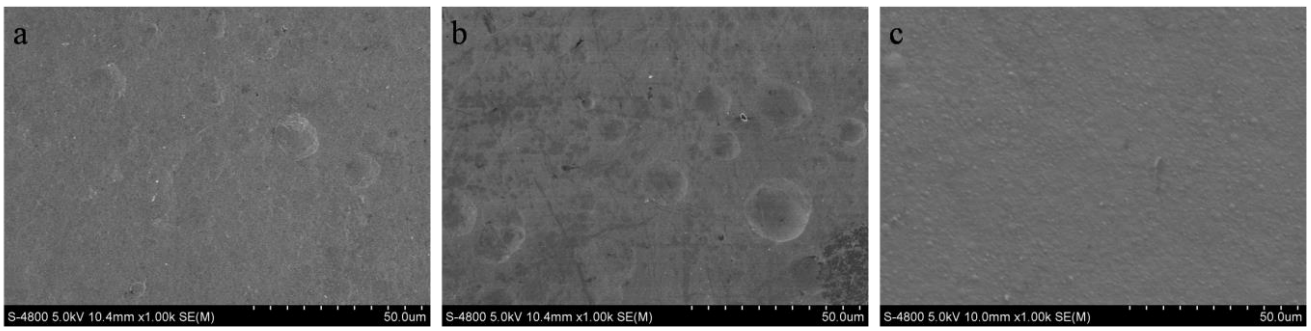

Figure 3. Surface morphology of coatings, a. 100/60(A/dm^2); b. 100/100(A/dm^2); c. 100/140(A/dm^2)

With the presence of microscopic bulges on the substrate surface and the rapid growth of preferential nucleation under high current density, large crystal cells and large bulges formed quickly on the surface of the deposited film. During electrodeposition, the electric field intensity of the convex regions was higher than that of other regions on the surface. Thus, the nickel ions in the plating solution were preferentially deposited in the convex regions, referred to as the “edge effect” (Fig.4a). As the deposition proceeded, the cellular bulges increased, whereas the other parts that grew slowly even were shielded, which led to a large number of defects on the coating surface and reduced the uniformity and density of the coating. To improve the surface quality of Ni coatings, Liu developed a controllable friction assistant method in jet electrodeposition [19]. Zhuo adopted a similar approach in his research [20]. However, the friction parameters must be appropriate, otherwise they would have an adverse effect on the coating. For interlaced jet electrodeposition, the electric field in the deposition area was redistributed after rotation because the power supply was turned off during the rotation, and

the direction of deposition was changed after rotation, which reduced the "edge effect" and increased the uniformity of the coating surface [12]. The periodic alteration of the electric field strength, together with the periodic redistribution of the electric field, induced the growing dots on the surface to break the growing inertia of the last layer, and regions shielded by large bulges would get growth again. This occurrence further weakened the "edge effect" and modified the growing defects of the last layer. The growing ability of each growing dot could be developed fully and evenly. This was in accordance with the previous study [21]. Meanwhile, the grain size and microstructure of the coatings varied under different current densities. The grain was refined as the current density increased [22, 23]. The change in current density for even layers could flatten the deposited odd layer surface, enhance the combination between layers, and improve the overall uniformity and density of the coating (Fig.4b). When the current density for even layers was decreased, the power line was redistributed and thinned, and the difference in electric field between large bulges and other regions was reduced, rendering the growth of the next layer more uniform. When the current density for even layers was increased, the increased overpotential could effectively refine the grain and improve the surface quality despite the increased difference in electric field.

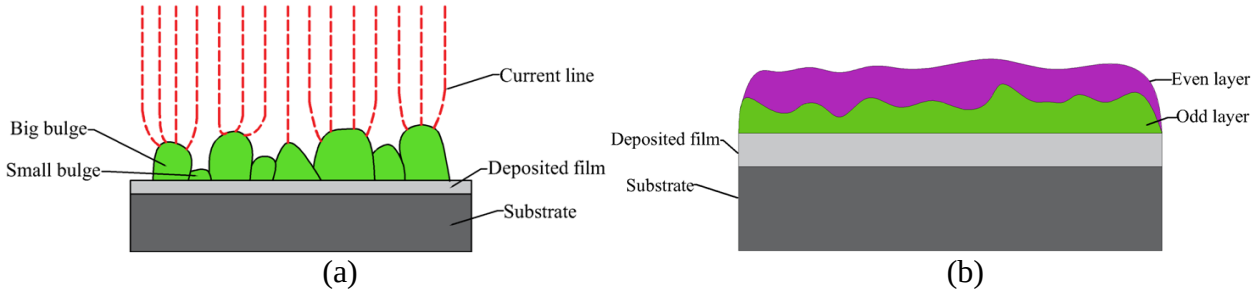

Figure 4. (a)Edge effect and its shielding (b) Leveling effect of even layer in gradient coating

3.2 Microstructure

Fig.5 presents the X-ray diffraction patterns of gradient multilayer nickel coatings prepared by interlaced jet electrodeposition. With reference to the standard Ni pattern, the corresponding crystal planes of the 3 diffraction peaks were (111), (200), and (220), and the coatings exhibited the face-centered cubic structure.

To quantify the crystallographic textures of the nickel coatings, the texture coefficient (TC) of (h k l) crystal planes in the XRD patterns were calculated according to the following formula [24]:

$$TC_{(hkl)} = \frac{I_{(hkl)}/I_{0(hkl)}}{\sum_{j=1}^{n} I_{(hkl)}/I_{0(hkl)}} \times 100\%$$

Where $I_{(hkl)}$ is the relative diffraction peak intensity of the (h k l) crystal planes of the coatings, $I_{0(hkl)}$is the intensity of standard nickel powder, and **n** is the number of peaks used in the calculation. In this case, (1 1 1), (2 0 0), and (2 2 0) peaks were used to calculate TC (**n** = 3). The results are listed in Table 3.

If the crystal planes have equal TCs, their orientation is disordered. If a crystal plane has a TC higher than the average value of 1/3, the crystal plane is the preferred orientation. The larger the TC is, the higher the degree of preferred orientation is. Table 3 shows that the preferred orientation of the coatings prepared under different current densities for even layers was (220). With an increase in current density for even layers, the degree of preferred orientation of the (220) crystal plane decreased, and the TCs of the (111) and (200) crystal planes increased. The TCs of the 3 crystal planes tended to be consistent.

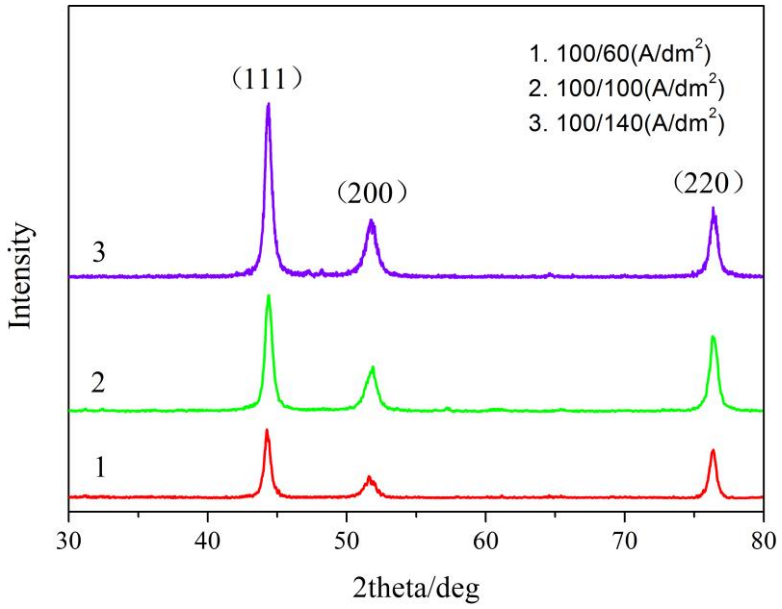

Figure 5. XRD patterns of Ni coatings

The results of this study were consistent with those of other studies. Pangarov stated that the preferred orientation of the grain in the coating was determined by the cathode overpotential [10]. In previous studies, researchers found that nickel plating appeared highly preferred orientation of (220) crystal plane under high current density [9, 10, 25], and the increase in TC of the (111) crystal plane contributed to grain refinement [26]. Pu found that as the pulse current density increased, the peak intensity of (111) crystal plane increased and the coating grain size decreased [27].

Table 3. $TC_{(hkl)}$ of crystal planes (%)

Sample number	(111)	(200)	(220)
1	19.8	13.4	66.8
2	20.3	18.2	61.5
3	29.1	19.7	51.8

3.3 Adhesion strength

The cross-sectional morphology of each of the 3 samples is shown in Fig.6. The samples were cut and then softly polished and rinsed with alcohol. The coating deposited at a constant current density of 100A/dm^2 was significantly separated from the substrate (Fig.6b). The coatings deposited at different current densities for even layers—60 and 140A/dm^2—showed a good combination with the NdFeB substrate, and the latter was better (Figs. 6a, 6c). The curves obtained using the automatic scratch tester showed that the adhesion strengths of the 3 coatings with the substrate were 18.1, 9.2, and 21.7N, respectively, as shown in Fig.7. The results demonstrated that with a change in current density for even layers, the adhesion strength between the coating and the substrate was markedly improved, which was consistent with the observation of the cross-sectional morphology.

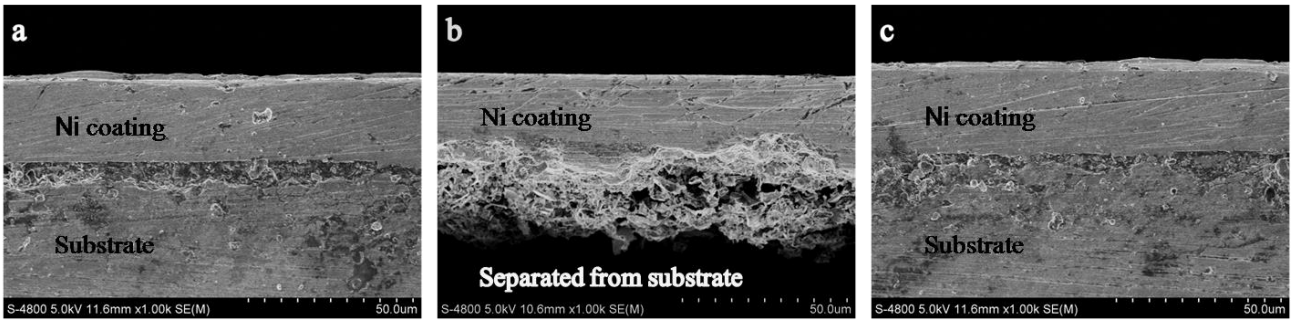

Figure 6. Cross-sectional morphology of Ni coatings on substrate, a. 100/60(A/dm^2); b. 100/100(A/dm^2); c. 100/140(A/dm^2)

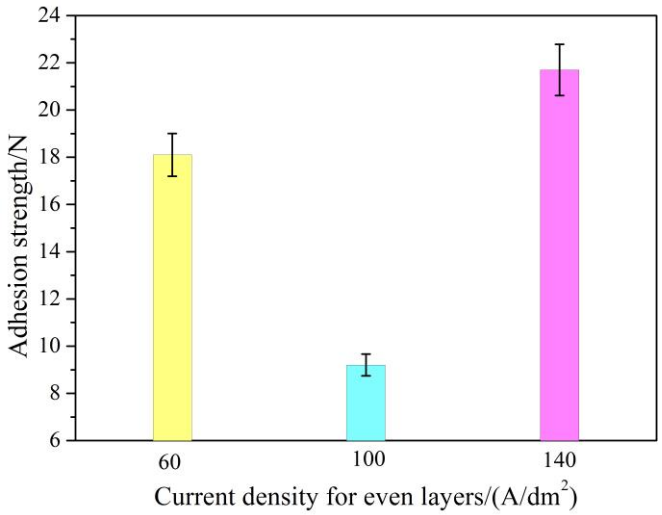

Figure 7. Adhesion strength of Ni coatings on substrate

During electrodeposition, the differences in lattice constant and thermal expansion coefficient between the coating and the substrate, as well as the presence of defects in the coating, led to residual

stress in the coating. Ziebell found that the residual stress arised in electrodeposited nanocrystalline nickel-tungsten coatings [28]. Li reviewed the cause for the residual stress in
nickel electrodeposition and analyzed the factors affecting the residual stress [29]. The residual stress accumulated continuously with an increase in coating thickness. The coating exhibited a tendency to crack, peel, or bulge if the residual stress was considerably high. During traditional jet electrodeposition, the coating was deposited with a reciprocating movement of the spay nozzle; thus, the residual stress of the coating varied considerably between the direction of scanning and the direction parallel to the scanning. In interlaced jet electrodeposition, the cyclic change in the direction of deposition could uniform the distribution of residual stress and regulate the increase of residual stress. With a periodic change in current density for different layers, the defects were significantly reduced, the uniformity and density of the coating were improved, and the structure of the multilayer coating became periodic gradient. These behaviors favored the reduction of residual stress. The microstructural difference between layers enhanced the staggered occlusion of interlayers and resulted in a good combination between layers in the gradient multilayer coating. Thus, the adhesion strength of the coating was markedly improved.

3.4 Microhardness

The microhardness of the coatings prepared under different current densities for even layers is shown in Fig. 8. When the current density for even layers was reduced from 100A/dm^2 to 60A/dm^2, the microhardness of the Ni coatings increased from 484HV to 514HV. When the current density was increased to 140A/dm^2, the microhardness was increased to 539HV, representing an increase of 11.36%. Tudela increased the microhardness of Ni coatings eledtrodeposited on Cu substrates to 360HV by adjusting the ultrasonic power [30]. The microhardness of Ni coating prepared by DC-jet electrodeposition reached 536HV in previous study [31]. Zhuo increased the microhardness to 546HV with movable and flexible fiction.

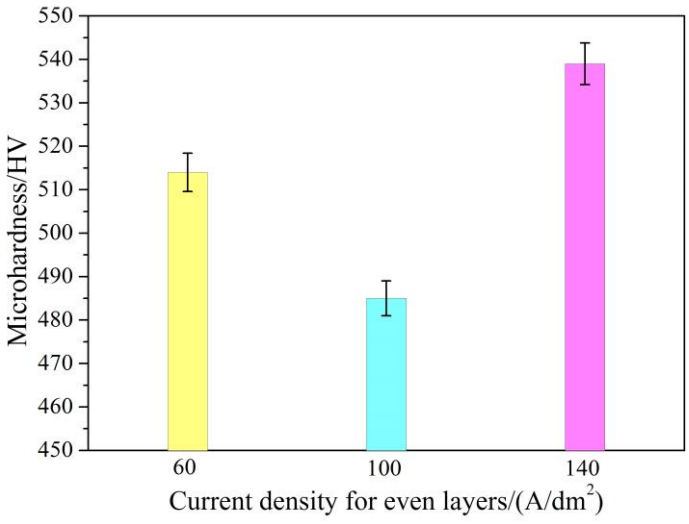

Figure 8. Microhardness of Ni coatings

The microhardness of the coating was related to its defects and structure. Analysis of surface morphology and adhesion strength led to the conclusion that with a change in current density for even layers, defects in the coating was reduced, the surface quality was improved, and the occlusal growth of interlayers improved the combination of layers and the coating structure. These improvements led to the increased uniformity and density of the coating and eventually strengthened the hardness of the coating. When the current density for even layers was increased, these beneficial effects became more apparent; thus, the prepared coating exhibited the highest microhardness.

3.5 Corrosion resistance

The potentiodynamic polarization curves of the pretreated NdFeB substrate and the 3 interlaced multilayer Ni coatings on the substrate in a 3.5wt%NaCl solution are presented in Fig.9a. The cathodic Tafel slope (b_c) and anodic Tafel slope (b_a) obtained by curve fitting, and the corrosion potential (E_{corr}) and corrosion current density (I_{corr}) calculated by Tafel extrapolation are listed in Table 4 [33–35].

As shown in Table 4, the NdFeB substrate had an extreme negative value of E_{corr} and its I_{corr} was considerably large. After plating multilayer nickel coatings on the NdFeB substrate, E_{corr} shifted to a considerably more positive value, and I_{corr} was reduced by 1 order of magnitude. These results indicated that the coatings exerted a substantial protective effect on the substrate. Compared with the conventional interlaced multilayer coating prepared under the constant current density, the gradient multilayer coatings prepared under periodically changed current density had a larger positive value of E_{corr}, and their I_{corr} was smaller. These 2 coatings exhibited higher corrosion resistance; the latter with increased current density for even layers showed the highest corrosion resistance. The electrochemical impedance spectroscopy measurements of the substrate and the 3 coatings were obtained in a 3.5wt% NaCl solution, shown as Nyquist plots in Fig.9b. The capacitive loop radius of the 3 three coatings was markedly larger than that of the substrate, and the radius of the gradient coating prepared under the current density of 100/140(A/dm^2) was the largest, suggesting the highest corrosion resistance. These findings were in agreement with the aforementioned results of potentiodynamic polarization curves.

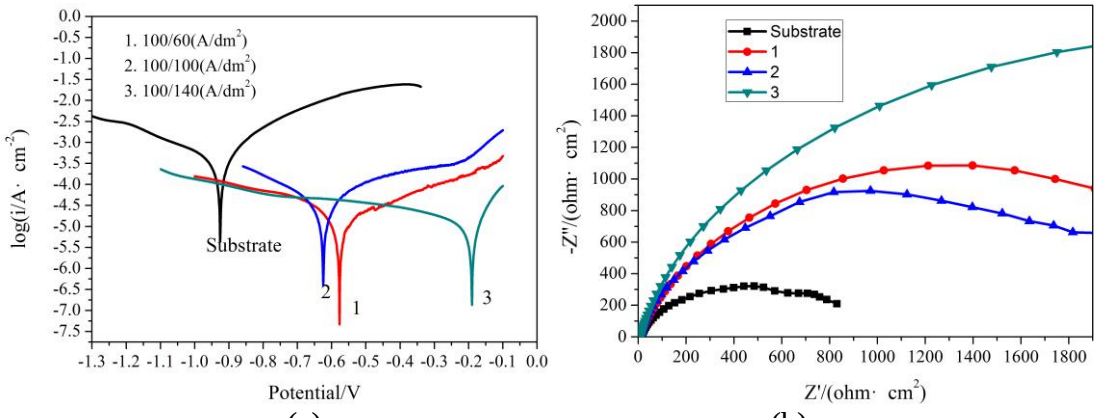

(a) (b)

Figure 9. (a) Potentiodynamic polarization curves (scan rate: 1mV/s) and (b) Nyquist plots of the substrate and Ni coatings (frequency range: 10^5–10^{-2}Hz)

Table 4. Corrosion potential and current density in 3.5wt% NaCl solution

Sample number	b_c/V·dec^{-2}	b_a/V·dec^{-2}	E_{corr}/V	I_{corr}/μA·cm^{-2}
Substrate	0.283	0.151	-0.926	382.31
1	0.231	0.394	-0.577	21.69
2	0.214	0.210	-0.625	52.11
3	0.363	0.104	-0.190	16.60

Zhang optimized the parameters of pulse electrodeposition and prepared a Ni coating with E_{corr} of -0.693V and I_{corr} of 16.3μA·cm^{-2} [36]. Zhu pointed out that the grain size and micro defects are two main factors that affected the corrosion resistance of nanocrystalline Ni coatings [37].The corrosive medium reached the substrate through the defects in coatings, causing corrosion failure [10]. Owing to the "edge effect" and its shielding, the coating deposited under 100/100(A/dm^2) had numerous defects on the surface, and its internal uniformity and density were relatively poor, rendering it vulnerable to corrosion. With the current density changed periodically, stress, defects, and microcracks were reduced, and coatings became smoother and more compact, thereby obstructing the corrosion path. In addition, the gradient structure and good combination between layers effectively mitigated the diffusion of corrosion to the substrate. Therefore, the corrosion resistance of periodic gradient coatings was improved.

4. CONCLUSIONS

(1) Periodically changing the current density can effectively weaken the "edge effect" and its shielding effect, increase the flatness of the coating surface, and improve the uniformity and density of the coating.

(2) Under high current density, the gradient interlaced multilayer coatings exhibited (220) preferred orientation. With the current density for even layers increased from 60A/dm^2 to 140A/dm^2, the TC of the (220) crystal plane decreased from 66.8% to 51.8%, and the TC of the (111) crystal plane increased from 19.8% to 29.1%.

(3) The periodic gradient design of interlaced multilayer coatings can reduce the coating defects and enhance the combination of layers. Compared with the conventional interlaced multilayer coating prepared under the current density of 100/100 (A/dm^2), the periodic gradient multilayer coatings prepared under the current density of 100/140 (A/dm^2) performed considerably better, the adhesion strength increased from 9.2N to 21.7N, the microhardness increased from 484HV to 539HV, and the corrosion current density decreased from 52.11μA·cm^{-2} to 16.60μA·cm^{-2}. The corrosion resistance was significantly improved.

ACKNOWLEDGEMENT
This work was supported by the National Natural Science Foundation of China (No.51475235, No. 51105204 and No.U1537105) and the Key Research and Development Plan of Jiangsu Province (BE2016010-3). We also extend our sincere thanks to all who contributed in the preparation of these instructions.

References

1. H.J. Kim, D.H. Kim, C.S. Koh, P.S. Shin, *IEEE T. Magn.*, 43 (2007) 2522.
2. W.L. Yan, S.H. Yan, D.B. Yu, J. Xu, H.C. Yang, Q.X. Hu, Y. Luo, *Met. Funct. Mater*., 15 (2008) 33.
3. C.F. Wei, J. Tang, L.R. Yang, D.W. Zhao, H. Lin, S.X. Deng, *Rare Met. Ceme. Carb*., 38 (2010) 47.
4. Y.W. Song, H. Zhang, H.X. Yang, Z.L. Song, *Mater. Corros*., 59 (2015) 1781.
5. W.J. Mo, L.T. Zhang, A.D. Shan, L.J. Cao, J.S. Wu, M. Komuro, *J. Alloy. Compd*., 461 (2008) 351.
6. T. Liu, L. Zhou, X.H. Cheng, X. Zhang, X.J. Yu, B. Li, *Met. Funct. Mater*., 18 (2011) 56.
7. A. Ali, A. Ahmad, K.M. Deen, *Mater. Corros*., 61 (2015) 130.
8. X. Yang, Q. Li, S. Zhang, H. Gao, F. Luo, Y. Dai, *J. Solid State Electr*., 14 (2010) 1601.
9. Y. Pan, S. Jiang, C.Y. Dai, T. Tang, Z.F. Zhou, Y.C. Zhou, *T. Nonferr. Met. Soc*., 17 (2007) 770.
10. Z.J. Tian, D.S. Wang, G.F. Wang, L.D. Shen, Z.D. Liu, Y.H. Huang, *T. Nonferr. Met. Soc*., 20 (2010) 1037.
11. L.D. Shen, Y.H. Wang, W, Jiang, X. Liu, C. Wang, Z.J. Tian, *Corros. Eng. Sci. Techn*., 52 (2017) 311.
12. L.D. Shen, C. Wang, Z.J. Tian, W. Jiang, W. Zhuo, K.L. Zhao, *Int. J. Electrochem. Sc*., 13 (2018) 1831.
13. H.Z. Wang, S.W. Yao, S. Matsumura, *Surf. Coat. Tech*., 157 (2002) 166.
14. E. García-Lecina, I. García-Urrutia, J.A. Díez, M. Salvo, F. Smeacetto, G. Gautier, R. Seddon, R. Martin, *Electrochim. Acta*, 54 (2009) 2556.
15. M.H. Allahyarzadeh, M. Aliofkhazraei, A.R. Sabour Rouhaghdam, V. Torabinejad, *J. Alloy. Compd*., 666 (2016) 217.
16. F. Yang, W. Tian, H. Nakano, H. Tsuji, S. Oue, H. Fukushima, *Mater. Trans*., 51 (2010) 948.
17. T. Sakamoto, K. Azumi, H. Tachikawa, K. Lokibe, M. Seo, N. Uchida, Y. Kagaya, *Electrochim. Acta*, 55 (2010) 8570.
18. A.M. Rashidi, A. Amadeh, *Surf. Coat. Tech*., 202 (2008) 3772.
19. X. Liu, L.D. Shen, M.B. Qiu, Z.J. Tian, Y.H. Wang, K.L. Zhao, *Surf. Coat. Tech*., 305 (2016) 231.
20. W. Zhuo, L.D. Shen, M.B. Qiu, Z.J. Tian, W. Jiang, *Surf. Coat. Tech*., 333 (2018) 87.
21. C. Wang, L.D. Shen, M.B. Qiu, Z.J. Tian, W. Jiang, *J. Alloy. Compd*., 727 (2017) 269.
22. M. Moravej, S. Amira, F. Prima, A. Rahem, M. Fiset, D. Mantovani, *Mater. Sci. Eng. B*, 176(2011)1812.
23. M. Bhardwaj, K. Balani, R. Balasubramaniam, A. Agarwal, *Surf. Eng*., 27(2014)642.
24. H. Matsushima, T. Nohira, I. Mogi, Y. Ito, *Surf. Coat. Tech*., 179 (2004) 245.
25. B. Lü, Z.F. Hu, X.H. Wang, B.S. Xu, *Chinese J. Nonferr. Met*., 24 (2014) 137.
26. L.P. Wang, S.H. Xiao, Y. Gao, H.W. Liu, T. Xu, *Plating & Finishing*, 27 (2005) 40.
27. N. Piao, J. Chen, Y.W. Sun, Z.X. Xu, X.M. Chen, X. Han, *Electroplating &Pollution Control*, 36(2016)4.
28. T.D. Ziebell, C.A. Schuh, *J. Mater. Res.*, 27(2012)1271.
29. Y.D. Li, X.X. Huang, Z.L. Yang, J. H. Yao, Y.X. Li, *Electroplating &Pollution Control*, 31(2011)4.
30. I. Tudela, Y. Zhang, M. Pal, I. Kerr, T.J. Mason, A.J. Cobley, *Surf. Coat. Tech*., 164 (2015) 49.
31. K.L. Zhao, L.D. Shen, M.B. Qiu, Z.J. Tian, W. Jiang, *Int. J. Electrochem. Sc.*, 12 (2017) 8578.
32. L.D. Shen, W. Zhuo, M.B. Qiu, W. Jiang, K.L. Zhao, C. Wang, *Mater. Sci. Tech.*, 34(2018)419.
33. F. Mansfeld, *Corros. Sci.*, 47(2005)3178.
34. X.L. Zhang, Z.H. Jiang, Z.P. Yao, Y. Song, Z.D. Wu, *Corros. Sci.*, 51(2009)581.
35. A.C. Murariu, N. Plesu, *Int. J. Electrochem. Sc.*, 10 (2015) 10832.
36. Y. Zhang, Y. Zhang, Q. Li, *Mater. Prot.*, 48(2015)19.

37. J. Zhu, L.D. Shen, Z.J. Tian, Z.D. Liu, Y.H. Huang, G.F. Wang, *Rare Met. Mater. Eng.*, 42(2013)2371.